

Orbital magnetic properties of quantum dots: the role of electron-electron interactions

L. G. G. V. Dias da Silva,¹ Caio H. Lewenkopf,² and Nelson Studart¹

¹*Departamento de Física, Universidade Federal de São Carlos, 13565-905 São Carlos SP, Brazil*

²*Instituto de Física, Universidade do Estado do Rio de Janeiro,
R. São Francisco Xavier 524, 20550-900 Rio de Janeiro, Brazil*

(Dated: November 20, 2018)

We study the magnetic orbital response of a system of N interacting electrons confined in a two-dimensional geometry and subjected to a perpendicular magnetic field in the finite temperature Hartree-Fock approximation. The electron-electron interaction is modelled by a short-range Yukawa-type potential. We calculate the ground state energy, magnetization, and magnetic susceptibility as a function of the temperature, the potential range, and the magnetic field. We show that the amplitude and period of oscillations in the magnetic susceptibility are strongly affected by the electron-electron interaction as evidenced in experimental results. The zero-field susceptibility displays both paramagnetic and diamagnetic phases as a function of temperature and the number of confined electrons.

PACS numbers: 73.21.La, 75.75.+a

I. INTRODUCTION

Much effort is currently devoted to the study of electron-electron interaction effects on the ground state and transport properties of mesoscopic and nanostructured devices.^{1,2,3} The theoretical analysis of small quantum dots, with $N \lesssim 8$ electrons, customarily employs sophisticated numerical tools.⁴ Those become computationally prohibitive for larger dots, that call for a more schematic approach, such as mean-field and/or semiclassical approximations. In this paper we address the specific question of how the electron-electron interactions change the magnetic susceptibility of quantum dots using the self-consistent Hartree-Fock approximation.

Our motivation stems mainly from the intriguing experimental data collected in the early 90's by Lévy and collaborators,⁵ who measured the orbital magnetic susceptibility of an array of mesoscopic squares lithographically inscribed in a GaAs/AlGaAs heterostructure. The authors found a surprisingly large paramagnetic susceptibility and a power law dependence of the zero-field susceptibility $\chi_0(B) \equiv \chi(B=0, T)$ with temperature. The first result is understood by means of a semiclassical single-particle analysis, showing that the magnetic susceptibility in ballistic devices is determined by the enclosed area and the stability of the shortest classical periodic orbits of the cavity.^{6,7,8,9,10,11} More specifically, the cavity geometry determines the classical periodic orbits relevant for $\chi(B, T)$, provided B is weak. For generic integrable systems such orbits come in families and the magnitude $\chi(B, T)$ scales as $k_F L$, where k_F is the wave number at the Fermi energy and L is the typical length scale of the cavity. In contrast, periodic orbits of chaotic systems are isolated and $\chi(B, T) \propto (k_F L)^{1/2}$. The semiclassical theoretical analysis also predicts an exponential decay for $\chi_0(T)$, which conflicts with the experimental data that display a much weaker temperature dependence. The experimental results⁵ raised natural and important questions, concerning the role of disorder and

interactions. These issues triggered interesting advances in the semiclassical approach. The disorder in the devices we are interested in is weak and long ranged, and hence dominated by small angle scattering. It was convincingly shown¹² that such kind of disorder has little influence on the semiclassical results derived for perfectly clean systems. A more far reaching and fundamental question is the role electron-electron interactions. In a sophisticated semiclassical approximation to the many-body problem, Ullmo and collaborators¹³ showed that interactions make $\chi(B, T)$ scale as $k_F L$ for integrable systems and $k_F L / \ln(k_F L)$ for chaotic ones. There two key approximations that allow for a full analytical treatment presented in Ref. 13. One approximation is to consider a zero-range residual interaction, that beclouds the exchange interaction, and the other is to give up self consistency.

Further motivation stems from a more recent experiment on the orbital magnetization of quantum-dot arrays¹⁴ that found a magnetization value two orders of magnitude larger than the one predicted by the noninteracting single-particle picture. Existing theoretical predictions based on the direct numerical diagonalization of the Hamiltonian for a few electrons^{15,16,17,18} and on a mean field approximation of the many-body problem¹⁹ indicated that the electron-electron interaction plays dominant role in the magnetic properties of quantum dots as clearly observed in the experiment.¹⁴

In this work, we resume the discussion on the influence of electron-electron interactions by studying the orbital magnetic response of a N -electron interacting system in a self-consistent Hartree-Fock (SCHF) approximation. The screened Coulomb electron-electron interaction is modelled by the short-range Yukawa potential $V(r) = V_0 e^{-\kappa r} / r$. Exact results are only known for the $N = 2$ case.^{17,18} The mean field approximation allows us to study systems up to $N \sim 40$ interacting electrons. Although the typical experimental dots in Refs. [5,14] have a much larger number of electrons, our study provides a

qualitative understanding of the interaction effects in the magnetic properties of the system.

We calculate the ground state energy E_g , magnetization, and magnetic susceptibility as a function of the relevant parameters of the system, namely, the temperature T , the potential range κ and the magnetic field B . Our results show discontinuities in $E_g(B)$ at $T = 0$, as previously reported.²⁰ These features are smoothed out for finite temperature.

We show that the magnetic response of a two-dimensional electronic cavity depends strongly on the electron-electron interaction and the magnetic susceptibility shows an oscillatory behavior similar to de Haas-von Alphen oscillations in metals. Furthermore, the amplitude and period of such oscillations are modified by the electron-electron interaction. We discriminate the kinetic, direct, and exchange contributions to the total magnetic susceptibility. The direct and exchange contributions also oscillate but with a different phase compared to the kinetic contribution. We also find that the susceptibility dependence on temperature and interaction strength displays non-universal features which are strongly dependent on the parameters. A slight enhancement of the zero-field susceptibility is seen as the number of electrons increases. The interaction-induced magnetic susceptibility shows paramagnetic and diamagnetic phases both as a function of temperature and interaction strength. A rather unexpected result is the behavior of the exchange interaction contribution to $\chi(B)$, which becomes larger than the direct contribution as the interaction strength increases.

The paper is organized as follows. In Sec. II we present the model system considered in this study and the mean field solution in the SCHF approximation. The main results are shown in Sec. III. Section IV brings the final remarks and conclusions. We also include an appendix where we present some specific details of the SCHF numerical implementation in the presence of discrete symmetries.

II. THE MODEL

We consider the problem of N two-dimensional (2D) interacting electrons in a confining potential subjected to an external magnetic field \mathbf{B} perpendicular to the electron system. Since we study the orbital contribution to the magnetization, we are allowed to simplify the problem and treat the electrons as spinless. The model Hamiltonian reads as

$$H = \sum_{n=1}^N h(\mathbf{r}_n) + \sum_{n < n'}^N v(\mathbf{r}_n, \mathbf{r}_{n'}), \quad (1)$$

where \mathbf{r}_n indicates the position of the n th electron. The single-particle Hamiltonian h is given by

$$h(\mathbf{r}) = \frac{1}{2m^*} \left[\mathbf{p} + \frac{e}{c} \mathbf{A}(\mathbf{r}) \right]^2 + u(\mathbf{r}), \quad (2)$$

where m^* is the electron effective mass. The vector potential \mathbf{A} is chosen in the symmetric gauge, namely, $\mathbf{A} = (-By/2, Bx/2, 0)$. The magnetic field is expressed in units of Φ/Φ_0 , where $\Phi = BA$ is the magnetic flux through the system area \mathcal{A} and $\Phi_0 = hc/e$ is the unit quantum flux. We choose the confining potential $u(\mathbf{r})$ as the 2D square well of side L that closely models the experiment.⁵

To account for screening effects the electron-electron interaction v is modelled by¹⁸

$$v(\mathbf{r}, \mathbf{r}') = \frac{e^2}{4\pi\epsilon_0\epsilon_r} \frac{e^{-\kappa|\mathbf{r}-\mathbf{r}'|}}{|\mathbf{r}-\mathbf{r}'|}, \quad (3)$$

where κ gives the effective interaction range and ϵ_r is the background dielectric constant. For $\kappa = 0$ there is no screening and the bare Coulomb interaction is recovered. Even though the $v(\mathbf{r}, \mathbf{r}')$ in Eq. (3) is different from the screened electron-electron interaction in the 2DEG when effects of the finite layer-thickness and image charges are taken into account,²¹ the Yukawa potential captures the main features of a more realistic interaction and has the advantage of being computationally more amenable to handle.²² We recall that the semiclassical approach is forced to use zero-range residual interaction in order to make the calculations feasible. By doing so, one loses a handle on the exchange interaction.

For a square dot of side L , the potential energy scales with $1/L$ while the kinetic energy scales with $1/L^2$. Hence, as L is increased, the potential energy becomes increasingly more important. It is then useful to introduce²⁰ an “effective strength” parameter L/a_B^* , where $a_B^* = \hbar^2(4\pi\epsilon_0\epsilon_r)/m^*e^2$ is the effective Bohr radius. The standard dimensionless parameter that quantifies the ratio between electronic potential and kinetic energies is r_s , that in 2D reads $r_s^2 = \mathcal{A}/(N\pi[a_B^*]^2)$. Hence, L/a_B^* and r_s are related as $r_s = (L/a_B^*)/\sqrt{\pi N}$. We consider here a range of parameters such that $1.5 < r_s < 2$, within the typical values of r_s in the experiments.^{5,14}

We calculate the ground-state energy in the SCHF approximation for finite temperatures. The SCHF equations read as^{23,24}

$$h(\mathbf{r})\phi_i(\mathbf{r}) + \sum_j \left[n_j \int d\mathbf{r}' \phi_j^*(\mathbf{r}') v(\mathbf{r}, \mathbf{r}') \phi_j(\mathbf{r}') \right] \phi_i(\mathbf{r}) - \sum_j \left[n_j \int d\mathbf{r}' \phi_j^*(\mathbf{r}') v(\mathbf{r}, \mathbf{r}') \phi_j(\mathbf{r}) \phi_i(\mathbf{r}') \right] = \varepsilon_i^{\text{HF}} \phi_i(\mathbf{r}), \quad (4)$$

where the sums run over all HF orbitals. Here $n_i = \{\exp[(\varepsilon_i^{\text{HF}} - \mu)/k_B T] + 1\}^{-1}$ is the Fermi occupation number of the i th HF orbital with corresponding wave function $\phi_i(\mathbf{r})$ and energy $\varepsilon_i^{\text{HF}}$. As standard, the chemical potential μ is determined by requiring that $N = \sum_i n_i$. We truncate the number of orbitals and take only the $M \approx 2N$ lowest energy states into account.

The SCHF ground state energy is given by

$$E_g^{\text{HF}} \equiv T^{\text{HF}} + V_d^{\text{HF}} - V_x^{\text{HF}}$$

$$= \sum_i n_i \langle \phi_i | h | \phi_i \rangle + \frac{1}{2} \sum_{i,j} n_i n_j \left(\langle \phi_i \phi_j | v | \phi_i \phi_j \rangle - \langle \phi_i \phi_j | v | \phi_j \phi_i \rangle \right), \quad (5)$$

where the $|\phi_i\rangle$ are the HF orbitals, self-consistent solutions of Eq. (4) and T^{HF} , V_d^{HF} and V_x^{HF} are the kinetic, direct and exchange contributions to the ground state energy respectively. Actually, it is numerically less expensive to compute E_g^{HF} as

$$E_g^{\text{HF}} = \frac{1}{2} \sum_i n_i \left(\varepsilon_i^{\text{HF}} + \langle \phi_i | h | \phi_i \rangle \right). \quad (6)$$

The calculations of the matrix elements were done numerically, with no further approximations other than setting the numerical precision. The number of elements grows as M^4 , where M is the basis size. For a typical calculation where we take $M \sim 50$, a numerical evaluation of about 10^7 four-dimensional integrals is required, a task far from trivial. To reduce that number, we have used an appropriate symmetrized basis on which the HF potential takes a block-diagonal form. Furthermore, we use properties of the Yukawa-like e-e interaction to reduce the four-dimensional integrals to a series of one-dimensional integrals on the relative polar angle. These steps are described in Ref. 18. Details on the HF numerical implementation in the presence of discrete symmetries are found in the Appendix.

III. SINGLE-PARTICLE PROPERTIES

The HF single-particle spectral properties play a major role for determining the system magnetization and magnetic susceptibility. In this section we present a general discussion of the model Hamiltonian single-particle spectrum that serves as a guide to interpret the magnetic results that follow.

Figure 1 shows the single-particle HF spectrum as a function of the magnetic flux Φ/Φ_0 for $N = 10$ electrons with $r_s = 1.22$ for $T = 0$ (left) and $T = \Delta$ (right). Here and throughout the manuscript Δ is the single-particle mean level spacing. Energy is given in units of $\hbar^2/(m^* L^2)$.

A very interesting feature displayed in Fig. 1 are the jumps in $\varepsilon_i^{\text{HF}}(B)$ for the $T = 0$ case. These discontinuities appear for other values of N as well and are related to sudden anti-crossings at Fermi energy, *i.e.*, involving the levels $\varepsilon_N^{\text{HF}}$ and $\varepsilon_{N+1}^{\text{HF}}$. For $T = 0$ the mean field selects the N lowest states. Hence, by parametrically moving through a level crossing, the character of the last occupied state is suddenly changed, and so is the mean-field. Narrow crossings, with a gap $\delta\varepsilon \ll \Delta$, that lead to sudden and very strong changes in the last occupied mean-field state, are responsible for the jumps.

The jumps disappear already for very low temperatures of the order of $k_B T \approx \delta\varepsilon \ll \Delta$, as illustrated in

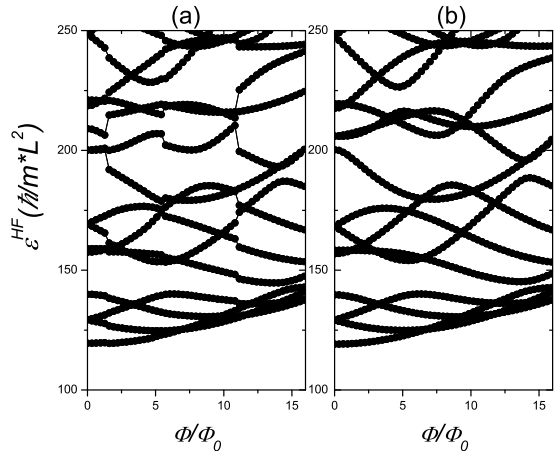


FIG. 1: Single-particle Hartree-Fock energy levels $\varepsilon_i^{\text{HF}}$ as a function of the magnetic flux Φ/Φ_0 for (a) $T = 0$ and (b) $k_B T = \Delta$. Here $N = 10$ and $r_s = 1.22$.

Fig. 1(b). For this reason, they are of very limited relevance for the experiments we are interested in, where $k_B T \gg \Delta$. However, Fermi energy anti-crossings explain similar features reported in the study of ground-state properties of quantum dots in the Coulomb blockade regime, that remained so far not understood.²⁰ Albeit also blurred by temperature, the later case deals with transport where the ground state many-body wave function matters and thus the Anderson orthogonality catastrophe can come into play.^{26,27}

IV. GROUND-STATE PROPERTIES

The magnetization $m(B)$ and the magnetic susceptibility $\chi(B)$ of an electronic cavity are obtained from

$$m(B) = -\frac{\partial \Omega}{\partial B} \quad \text{and} \quad \chi(B) = -\frac{1}{L^2} \frac{\partial^2 \Omega}{\partial B^2}. \quad (7)$$

In turn, the grand canonical potential Ω is directly computed from the ground state HF energy by $\Omega = E_g^{\text{HF}} - TS - N\mu$, where S is the entropy and μ the chemical potential, both functions of B .

In the remaining of the paper, the magnetization is given in units of the effective Bohr magneton $\mu_B^* = e\hbar/2m^*c$ and the magnetic susceptibility is expressed in units of the Landau susceptibility, namely $|\chi_L| = e^2/(12\pi m^*c^2)$. For simplicity, the non-interacting case is referred to as “ $L/a_B^* = 0$ ”.

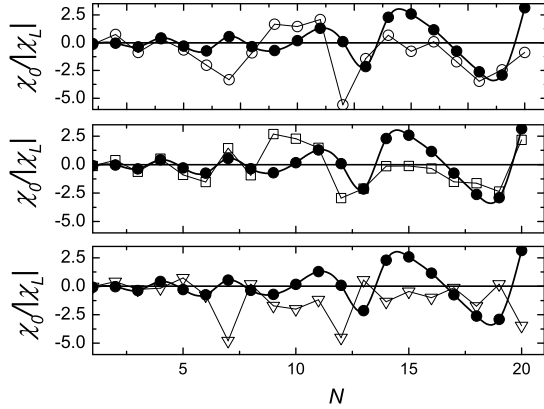


FIG. 2: Top panel: zero-field susceptibility χ_0 as a function of the particle number N for the non-interacting (thick solid line with filled circles) and $r_s = 1.5$ (open circles) cases at $k_B T = \Delta/2$. Middle panel: the same for the kinetic term (open squares). Bottom panel: the same for the exchange contribution (open triangles) to the magnetic susceptibility.

A. Exchange contribution

Following Eq. (5), one can distinguish different contributions to the magnetic susceptibility, namely

$$\chi = \chi^{\text{kin}} + \chi^{\text{d}} + \chi^{\text{x}} \quad (8)$$

arising from the kinetic, direct, and exchange interaction terms of the HF ground state energy $E_g^{\text{HF}}(B)$. As shown below, it is instructive to compare the later with the susceptibility computed for non-interacting electrons in a square cavity, $\chi^{\text{non-int}}$.

The zero-field susceptibility $\chi_0(T) \equiv \chi(B=0, T)$ is obtained for different N up to $N=20$ at $k_B T = \Delta/2$. The results are shown on Fig. 2. The noninteracting susceptibility $\chi^{\text{non-int}}$ (filled circles) oscillates with increasing amplitude as N is varied (or equivalently, as a function of $k_F L$). This is in agreement with the previous semiclassical calculations.^{6,7,8,9} As we include the electron-electron interaction included, keeping $r_s \approx 1.5$ for all N , the interacting susceptibility (open circles) sensibly deviates from the noninteracting case. We find that such deviations are mainly caused by the exchange contribution to the susceptibility. While the kinetic contribution (squares) resembles the noninteracting situation, the exchange term (triangles) exhibits rather large fluctuations, which are the main responsible for the deviations in the total interacting susceptibility.

The exchange contribution to the susceptibility increases with the interaction strength L/a_B^* and is already of the order of the kinetic contribution for $r_s \approx 1.5$. This is illustrated in Fig. 3, where we chose a maximum of the noninteracting $\chi_0^{\text{non-int}}(N)$, namely, $N=20$ and vary L/a_B^* . For low values of L/a_B^* , the paramagnetic kinetic term χ^{kin} (filled squares) dominates and stays almost

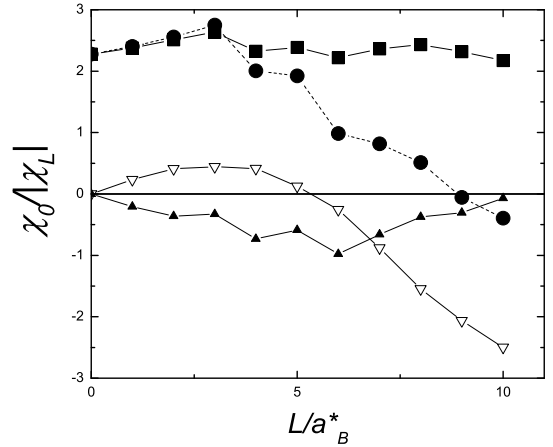


FIG. 3: Zero-field susceptibility χ_0 (circles) as a function of interacting strength L/a_B^* for $N=20$ electrons and $k_B T = \Delta/2$. Kinetic (squares), direct interaction (filled triangles), and exchange interaction (empty triangles) contributions to χ_0 are shown for comparison.

constant while the total susceptibility decreases. This behavior of the total susceptibility is dictated by the exchange term χ^{x} , which is initially of the order of the direct contribution. As the interaction strength increases, both the absolute value of the direct and exchange terms increase. It is interesting to notice that χ^{x} overcomes χ^{d} for $L/a_B^* \approx 5$ ($r_s \approx 0.63$) and is of the same order as the kinetic term for $L/a_B^* \approx 10$ ($r_s \approx 1.26$).

This is a somewhat unexpected result, since the direct contribution V_d^{HF} to the ground state energy is 3 to 4 times *larger* than the exchange contribution V_x^{HF} in this range of r_s . It turns out, however, that the magnetic V_x^{HF} is more sensitive to variations of the magnetic field than V_d^{HF} , giving rise to the larger exchange contribution.

B. Magnetic field effects

The electron-electron interaction also induces some nontrivial effects in the magnetic field dependence of both the magnetization and the magnetic susceptibility. The results for $m(B)$ and $\chi(B)$ in the Coulomb ($\kappa=0$) case are shown in Figs. 4 and 5 for different N and L/a_B^* . In this subsection we take $k_B T$ of the order of Δ , to wash out effects due to level crossings, while preserving the quantum effects due to long energy range spectral correlations.

In the noninteracting case, the magnetization curves for different N values are very similar. For low fields, small oscillations arise and, as Φ increases, a positive magnetization phase appears. When the interaction between the electrons is included, the magnetization curves for $N=10$ and $N=20$ are quite different (see Fig. 4). In particular, for $L/a_B^* = 10$, the orbital magnetization

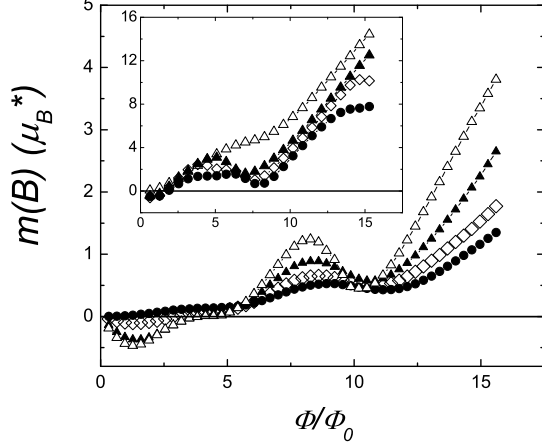


FIG. 4: Magnetization $m(B)$ as a function of $B = \Phi/L^2$ for $L/a_B^* = 0$ (circles), 2 (diamonds), 5 (filled triangles), and 8 (open triangles). Here $N = 10$ and $k_B T = \Delta$. Inset: $N = 20$ for $L/a_B^* = 0$ (circles) 3 (diamonds), 5 (filled triangles), and 10 (open triangles) at $k_B T = \Delta/2$.

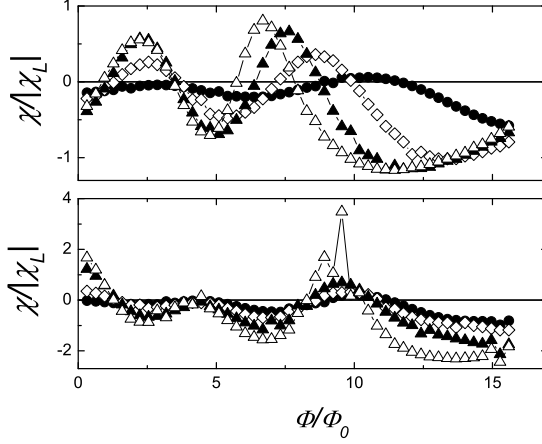


FIG. 5: Magnetic susceptibility $\chi/|\chi_L|$ as a function of the magnetic flux for $N = 5$ (top) and $N = 10$ (bottom) with $L/a_B^* = 0$ (circles), 2 (diamonds), 4.7 (filled triangles), and 8 (open triangles). The temperature is $k_B T = \Delta$.

is about four times larger for $N = 20$ than for $N = 10$. This suggests that large systems can display strong orbital magnetization effects, in line with the experimental results.¹⁴

For $N = 5$, a clear oscillatory behavior is seen on $\chi(B)$ (see top of Fig. 5). The amplitudes are of order $|\chi_L|$ and, as the interaction strength is increased, both the amplitude and frequency also increase. This behavior is similar to the de Hass-von Alphen effect observed in metals. In that case, both the amplitude and frequency of $\chi(B)$ oscillations are proportional to the chemical potential of

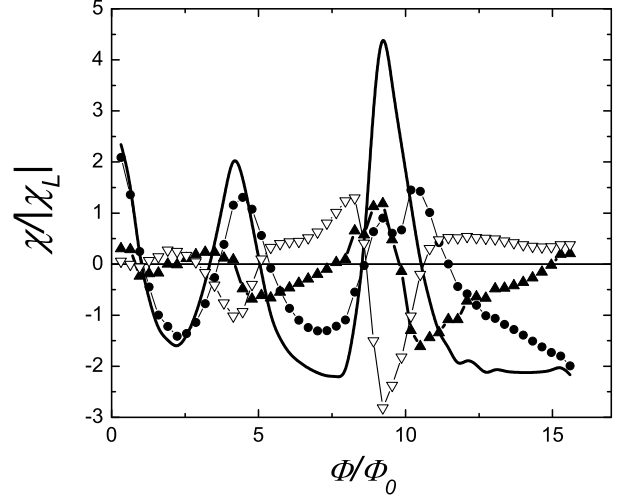


FIG. 6: Magnetic susceptibility χ/χ_L (thick solid line) as a function of Φ/Φ_0 for $N = 10$ at $k_B T = \Delta/2$ and $L/a_B^* = 5.0$. The symbols correspond to the kinetic (circles), direct (filled triangles) and exchange contributions (open triangles).

the system. In the single-particle effective potential approximation, an increase in the interaction strength is equivalent to an increase in the effective chemical potential of the HF levels, which corroborates the analogy.

The oscillations are modified with increasing number of particles, see bottom panel of Fig. 5. For larger values of L/a_B^* , $\chi(B)$ displays fluctuations near $\Phi/\Phi_0 = 10$ due to crossings between the Hartree-Fock single-particle states at the Fermi level, as discussed in Sec. III. Notice that although the level crossing jumps in the single-particle spectrum seem to have already disappeared at $k_B T = \Delta$, see Fig. 1, they are greatly enhanced in $\chi(B)$, due the second derivative in Eq. (7).

We observe that the exchange part plays an important role to for the computation of the B dependence on the magnetic susceptibility χ . In Fig. 6 all contributions are shown as a function of Φ/Φ_0 for a lower temperature, namely $k_B T = \Delta/2$ and $r_s = 0.9$. The pronounced paramagnetic peak around $\Phi/\Phi_0 \approx 10$ (also observed at the bottom panel of Fig. 5) is mainly due to the exchange contribution χ^x . Notice that frequently χ^d and χ^x give contributions of opposite signs appears as Φ/Φ_0 is varied.

It is worth mentioning that these results are somewhat different from the ones obtained by the exact diagonalization for the two-electron case,¹⁸ where the electron spin plays an important role on the orbital properties of the system. In that situation, singlet-triplet transitions give rise to low-temperature peaks of about $3|\chi_L|$ of magnitude in the orbital susceptibility but no oscillatory behavior is found on $\chi(B)$. Also, the magnetization $m(B)$ in the exact $N = 2$ case is always negative, even in the large field regime.

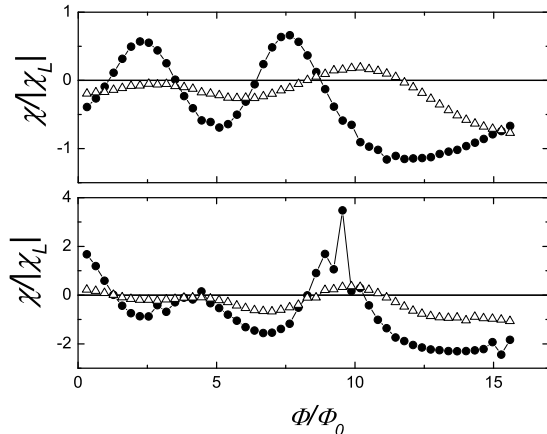


FIG. 7: Magnetic susceptibility $\chi(B)$ for different interaction ranges (Coulomb [circles] and $\kappa^{-1} = L/10$ [triangles]) for $N = 5$ (top) and $N = 10$ (bottom).

In Fig. 7, we compare the susceptibilities in the case of Coulomb and short-range potentials. In order to get a qualitative comparison, we consider the strong-screening regime, using $\kappa^{-1} = L/10$.

In this short-range limit, the interaction between the electrons is exponentially suppressed for distances larger than the screening length κ^{-1} and the overall magnetic response, which is averaged over the whole dot, is then similar to the noninteracting case. This can be clearly seen in Fig. 7 where the curves for $\kappa^{-1} = L/10$ are quite similar to those for $L/a_B^* = 0$ depicted in Fig. 5, showing that the shielding of the electron-electron interaction is quite effective and a noninteracting picture is a good approximation for the thermodynamic properties of the system.

For such low screening lengths, the Fermi wavelength $\lambda_F \sim \pi L/\sqrt{N}$ is larger than κ^{-1} by one order of magnitude. In the regime $\lambda_F \gg \kappa^{-1}$, the 2D screened interaction can be well approximated by a δ -type contact interaction.¹³ Our results show that the noninteracting picture captures the main features of such approximation in the Hartree-Fock scheme. Therefore, one has to consider larger screening lengths in order to see residual interaction effects in the magnetization and magnetic susceptibility.

C. Temperature dependence

The zero-field susceptibility decays with temperature, as expected, but the decay rate is rather large. For $k_B T/\Delta = 3$, χ_0 is already negligible compared to the $T = 0$ value (see Fig. 8). In the intermediate range of $k_B T \sim \Delta$, non-universal features arise. As an example, the inset of Fig. 8 shows our result for a dot with $N = 5$ electrons: $\chi_0(T)$ is negative (except for $T \sim 0$)

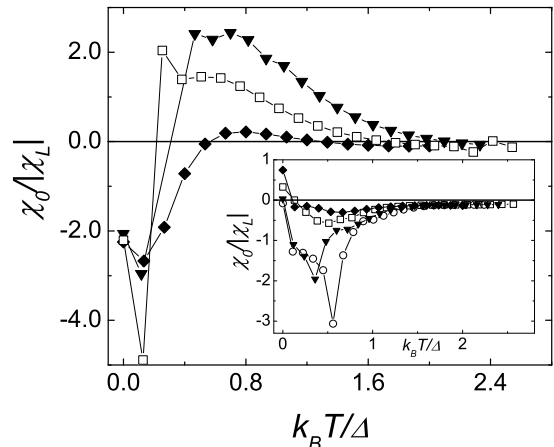


FIG. 8: Temperature dependence of the zero-field susceptibility $\chi_0(T)$ for $N = 10$ and $L/a_B^* = 0$ (diamonds), 2 (squares) and 5 (triangles). In the inset, the same is shown for $N = 5$ with an additional curve for $L/a_B^* = 8$ (circles).

and has pronounced minima at $k_B T = \Delta/2$, even in the non-interacting case. For $N = 10$, $\chi_0(T)$ displays both positive (for $k_B T < 0.4\Delta$ and $k_B T > \Delta$) and negative values ($0.4\Delta < k_B T < \Delta$), indicating a diamagnetic-paramagnetic transition. In both cases, the interaction-induced susceptibility, $\chi - \chi^{\text{non-int}}$, is positive, indicating a paramagnetic contribution due to the electron-electron interaction.

Such a diamagnetic-paramagnetic transition for increasing N is in agreement with previous theoretical results. For $N = 2$, exact diagonalization results¹⁸ show that $\chi_0(T)$ is diamagnetic for a temperature range up to 10Δ . On the other hand, semiclassical analysis^{6,7,9} suggests a paramagnetic $\chi_0(T)$ for $N \sim 100$. Therefore, a diamagnetic-paramagnetic transition is expected in the intermediate particle number regime.

V. CONCLUDING REMARKS

We have considered the ground-state properties of a system of N interacting electrons confined in a 2D geometry and subjected to a perpendicular magnetic field in the finite temperature SCHF approximation. The magnetic susceptibility was calculated as a function of the relevant parameters of the system (magnetic field, number of electrons, temperature, and strength and range of the particle interaction). The ground-state energy was obtained for both the Coulomb interaction and the short-range Yukawa potential.

Our results show that the electron-electron interaction introduces nontrivial effects in the magnetic properties of the system. The magnetic susceptibility shows de Hass-van Alphen-like oscillations which are enhanced as the interaction strength increases. The magnetization in-

creases when more electrons are added in the dot, which indicates that a strong orbital magnetization should be expected for larger systems. For a higher number of electrons, new features arise, including strong diamagnetic fluctuations as a function of the magnetic field.

The zero-field susceptibility $\chi_0(T)$ shows both paramagnetic and diamagnetic phases as a function of the temperature. We found that $\chi_0(T) \rightarrow 0$ as T increases and the susceptibility induced by interaction is positive, yielding a paramagnetic contribution to χ_0 irrespective of the value of N . However, non-universal N -dependent features appear in the intermediate temperature range of $k_B T \approx \Delta$.

Acknowledgments

This work was supported by Brazilian funding agencies FAPESP, CNPq, PRONEX, and by the Instituto do Milênio de Nanociências. CHL thanks Centro Brasileiro de Pesquisas Físicas for the hospitality. We thank M. A. M. de Aguiar, F. Toscano, and R. O. Vallejos for helpful discussions.

APPENDIX A: HARTREE-FOCK EQUATIONS IN MATRIX FORM

We solve the HF self-consistent equations (4) iteratively by diagonalization. The eigenfunctions of the square billiard of side length L , namely

$$\varphi_\alpha(x, y) = \frac{2}{L} \sin\left(\frac{m\pi}{L}x\right) \sin\left(\frac{n\pi}{L}y\right). \quad (\text{A1})$$

where $\alpha \equiv (m, n)$, separated into the square four point symmetry classes, form the basis set $\{\psi_\alpha\}$. The later are also eigenbasis of the operator $R_{\pi/4}$ that rotates the coordinates by $\pi/4$. The eigenvalues $R_{\pi/4}$, namely $c_\alpha = +1, -1, +i$ and $-i$, label the square billiard symmetry classes. More details can be found in Ref. 18.

The bottleneck for HF method is the calculation of the two-body electron interaction integrals, namely

$$I_{\alpha\gamma\beta\delta} \equiv \int d\mathbf{r} \int d\mathbf{r}' \psi_\alpha^{c_\alpha*}(\mathbf{r}) \psi_\gamma^{c_\gamma*}(\mathbf{r}') v(\mathbf{r}, \mathbf{r}') \psi_\beta^{c_\beta}(\mathbf{r}) \psi_\delta^{c_\delta}(\mathbf{r}'). \quad (\text{A2})$$

Here the advantage of separating the basis into symmetry classes comes into play. Many of the matrix elements $I_{\alpha\gamma\beta\delta}$ are zero, depending on the single-particle symmetry classes involved. The “selection rule” can be summarized as follows: given the single-particle symmetry class of the states $\psi_\alpha^{c_\alpha}, \psi_\beta^{c_\beta}, \psi_\gamma^{c_\gamma}$, and $\psi_\delta^{c_\delta}$, the matrix element $I_{\alpha\gamma\beta\delta}$ will be only nonzero if¹⁸

$$c_\alpha \otimes c_\beta = c_\gamma \otimes c_\delta. \quad (\text{A3})$$

Therefore, only states with the same two-particle symmetry class are coupled by the interaction potential.

Let us now express the HF equations in terms of the two-body residual interaction integrals I . The HF orbital wave functions read

$$\phi_i(\mathbf{r}) = \sum_{\alpha=1}^M C_{i\alpha} \psi_\alpha^{c_\alpha}(\mathbf{r}). \quad (\text{A4})$$

We typically truncate the basis set taking at least the $M = 50$ lowest square billiard energy states. The roman labels refer to the HF orbitals ϕ , whereas the greek ones to the basis set ψ . The resulting matrix form of Eq. (4) is

$$\sum_{\beta} (h_{\alpha\beta} + v_{\alpha\beta}^{\text{HF}}) C_{i\beta} = \varepsilon_i^{\text{HF}} C_{i\alpha}. \quad (\text{A5})$$

Here $v_{\alpha\beta}^{\text{HF}} = v_{\alpha\beta}^{\text{d}} - v_{\alpha\beta}^{\text{x}}$, that are given by

$$\begin{aligned} v_{\alpha\beta}^{\text{d}} &= \int d\mathbf{r} \int d\mathbf{r}' \rho(\mathbf{r}', \mathbf{r}') \psi_\alpha^{c_\alpha*}(\mathbf{r}) v(\mathbf{r}, \mathbf{r}') \psi_\beta^{c_\beta}(\mathbf{r}) \\ v_{\alpha\beta}^{\text{x}} &= \int d\mathbf{r} \int d\mathbf{r}' \rho(\mathbf{r}, \mathbf{r}') \psi_\alpha^{c_\alpha*}(\mathbf{r}) v(\mathbf{r}, \mathbf{r}') \psi_\beta^{c_\beta}(\mathbf{r}'), \end{aligned} \quad (\text{A6})$$

with the density matrix ρ given by

$$\rho(\mathbf{r}, \mathbf{r}') = \sum_{i=1}^M n_i \phi_i(\mathbf{r}) \phi_i^*(\mathbf{r}'), \quad (\text{A7})$$

where n_i is the Fermi occupation number of the i th HF orbital. Notice that since ρ does not distinguish different symmetry classes, the HF mean field can effectively mix them. Hence, the HF potential reads

$$v_{\alpha\beta}^{\text{HF}} = v_{\alpha\beta}^{\text{d}} - v_{\alpha\beta}^{\text{x}} = \sum_{\gamma=1}^M \sum_{\delta=1}^M D_{\gamma\delta} (I_{\alpha\gamma\beta\delta} - I_{\alpha\gamma\delta\beta}), \quad (\text{A8})$$

where, by introducing

$$D_{\gamma\delta} \equiv \sum_{i=1}^M n_i C_{i\gamma}^* C_{i\delta}. \quad (\text{A9})$$

we eliminate one sum over the single-particle orbitals. The computation of (A8) is speed up by exploring the sparse nature of $I_{\alpha\gamma\delta\beta}$.

Notice that the HF potential matrix elements will be, in the general case, complex numbers since the basis itself is complex. The remaining of the numerical implementation is very standard. The convergence of the ground-state energies is obtained at iteration n if $|E_{n+1}^{\text{HF}} - E_n^{\text{HF}}|/E_n^{\text{HF}} < 10^{-5}$.

-
- ¹ L. L. Sohn, L. P. Kowenhoven and G. Schon, eds., *Mesoscopic Electron Transport* (Kluwer, New York, 1997).
 - ² I. L. Aleiner, P. W. Brouwer, and L. I. Glazman, Phys. Rep. **358**, 309 (2002).
 - ³ D. Ullmo and H. U. Baranger, Phys. Rev. B **64**, 245324 (2001).
 - ⁴ S. M. Reimann and M. Manninen, Rev. Mod. Phys. **74**, 1283 (2002).
 - ⁵ L. P. Lévy, D. H. Reich, L. Pfeiffer, and K. West, Physica B **189**, 204 (1993).
 - ⁶ S. D. Prado and M. A. M. de Aguiar, J. P. Keating and R. Egidio de Carvalho J. Phys. A **27**, 6091 (1994).
 - ⁷ F. von Oppen, Phys. Rev. B **50**, 17151 (1994).
 - ⁸ O. Agam, J. Phys. I **4**, 697 (1994).
 - ⁹ D. Ullmo, K. Richter, and R. A. Jalabert, Phys. Rev. Lett. **74**, 383 (1995); K. Richter, D. Ullmo, and R. A. Jalabert, Phys. Rep. **276**, 1 (1996).
 - ¹⁰ E. Gurevich and B. Shapiro, J. Phys. I **7**, 807 (1997).
 - ¹¹ M. O. Terra, M. L. Tiago, M. A. M. de Aguiar, Phys. Rev. E **58** 5146 (1998).
 - ¹² K. Richter, D. Ullmo, and R. A. Jalabert, Phys. Rev. B **54**, R 5219 (1996); J. Math. Phys. **37**, 5087 (1996).
 - ¹³ D. Ullmo, H. U. Baranger, K. Richter, F. von Oppen, and R. A. Jalabert, Phys. Rev. Lett. **80**, 895 (1998).
 - ¹⁴ M. P. Schwarz, D. Grundler, M. Wilde, Ch. Heyn, and D. Heitman, J. Appl. Phys. **91**, 6875 (2002).
 - ¹⁵ P. A. Maksym and T. Chakraborty, Phys. Rev. B **45**, 1947 (1992).
 - ¹⁶ M. Wagner, U. Merkt, and A. V. Chaplik, Phys. Rev. B **45**, 1951 (1992).
 - ¹⁷ C. E. Creffield, J. H. Jefferson, S. Sarkar, and D. L. J. Tipton, Phys. Rev. B **62**, 7249 (2000).
 - ¹⁸ L. G. V. Dias da Silva and M. A. M. de Aguiar, Phys. Rev. B **66**, 165309 (2002).
 - ¹⁹ M. M. Fogler, E. I. Levin, and B. I. Shklovskii, Phys. Rev. B **49**, 13767 (1994).
 - ²⁰ K.-H. Ahn, K. Richter, and I.-H. Lee, Phys. Rev. Lett. **83**, 4144 (1999).
 - ²¹ T. Ando, A. B. Fowler, and F. Stern, Rev. Mod. Phys. **54**, 437 (1982).
 - ²² L. Candido, J.-P. Rino, N. Studart, and F. M. Peeters, J. Phys.: Condens. Matter **10**, 11627 (1998).
 - ²³ H. Tamura and M. Ueda, Phys. Rev. Lett. **79**, 1345 (1997).
 - ²⁴ D. J. Dean, M. R. Strayer, and J. C. Wells, Phys. Rev. B **64**, 125305 (2001).
 - ²⁵ D. Pfannkuche, V. Gudmundsson, and P. A. Maksym, Phys. Rev. B **47**, 2244 (1993).
 - ²⁶ R. O. Vallejos, C. H. Lewenkopf, and Y. Gefen, Phys. Rev. B **65** 085309 (2002).
 - ²⁷ Y. Gefen, R. Berkovits, I. V. Lerner, and B. L. Altshuler, Phys. Rev. B **65**, 081106 (2002).